KSME Journal, Vol. 7, No. 3, pp. 272~281, 1993

Wave Transmission at Discontinuities Using Wavenumber-Frequency Techniques

Segye Oh*

(*Received February 23, 1993*)

The problem of wave transmission between two finite beams joined by a cross beam welded between them is solved taking full account of longitudinal and flexural waves in all the beams. Prediction of longitudinal and flexural wave transmission through the "T" joints in the beam system was performed over a wide band frequency range. The wavenumber-frequency spectrum was used to separate the wave types based on their different dispersive characteristics. Flexural direction forces at one end of the beam system were examined. The experimental data were taken using an accelerometer array and a simultaneous twenty-three channel measuring system. A transfer function correction technique was employed to account for the instrumentation errors. Experimental results were confirmed by the finite element analysis results. The total mean squared vibrational energy levels were calculated in each section of the beam system to quantify the transmission characteristics of both flexural and longitudinal waves passing through the beam joints.

Key Words: Dispersion, Nyquist-Wavenumber, Wavenumber-Frequency, Zero-Padded

1. Introduction

The problems related to structural vibration concern vibration control measures to be taken to reduce the amount of mechanical energy being transported by structural waves, so that the vibration of the structure is reduced. As a complementary measure, attempts can be made to observe the mechanical energy along its propagation paths in some convenient way before it reaches the regions where it is radiated into the surroundings. It is therefore of great importance to determine the dominant paths of vibration propagation through the structure.

The elementary theory of vibrational energy transmission is largely based on a model of lumped masses interconnected through spring and dashpots. Yoshimura(1977, 1979) identified the joint stiffness and joint damping coefficients in linear spring-dashpot models. Gaul(1983) identified the rigidity and the damping in a spring-dashpot model using the concept of equivalent linearization. This approximation was found to be satisfactory for the behavior of the structure at low frequencies, but not at high frequencies. Lyon(1975) proposed a similar approach known as the Statistical Energy Analysis technique, in which the system may be subdivided into subsystems as lumped units, with input and output power proportional to its energy. The Statistical Energy Analysis technique may give the estimated value based on the averaged behavior for many kinds of problems. Bhattacharya(1971) in the investigation of wave transmission through a plate connecting two infinite parallel plates has shown that the reflecting wave fields on the cross piece must be considered which will give rise to resonance. Rosenhouse(1970) had described the "black box approach" used for wave transmission in finite systems containing multi-joints. This approach has been confined to prob-

* Agency for Defense Development, Taejeon 305-606, Korea

lems in which only bending and longitudinal waves are generated. This method was developed on the basis of the Bernoulli-Euler theory of a beam. Doyle and Kamle(1987) investigated the behavior of flexural waves in the presence of a "T" joint for a finite beam system.

Much work has been done on wave transmission at joints for an infinite system or for a finite system with single joint. In practical situations, the structure is a finite system and has more than one joint. This study is an extension of previous works and investigates wave transmission of a finite system which consists of two parallel beams of finite length connected by a cross beam, taking full account of flexural and longitudinal waves in all the beams. The experimental and numerical results are represented as wavenumber-frequency spectra.

The wavenumber-frequency spectrum was proposed as a method for direct measurement of the wall pressure fluctuations in a turbulent boundary layer by Maidanik and Jorgensen(1967). Blake and Chase(1971), Bull(1967), and Wills (1970) used this technique to perform such measurements. The successful ability to measure the wavenumber-frequency characteristics of space-time fields demonstrated that this technique could be a powerful tool for interpretation and analysis of experimental data.

In spite of the use of wavenumber-frequency analysis for study of the wave fields produced by turbulent flow over the surfaces, the applications in structural waves are less widespread. The goal of the present work is to develop an experimental technique for spatial decomposition of structural waves using the wavenumber-frequency spectrum method.

2. Numerical Analysis

2.1 Description of finite element modeling of an "H" frame

The model shown in Fig. 1 consists of five steel beam sections in order to know what portion of energy is transmitted and what portion of energy is attenuated when the longitudinal and the flexural waves pass through the joints. The lengths of each beam section of the system are $L_1=6.5$ feet, $L_2=4.5$ feet, $L_3=6$ feet, $L_4=5$ feet and $L_5=4$ feet.

In order to investigate wave transmission through two "T" joints using the finite element method, the three dimensional beam element was chosen which has six degrees of freedom at each node : translation in the nodal x, y, and z directions and rotations about the nodal x, y, and z axis. The element size of 1.375 inch is employed in this study which is the same as the accelerometer spacing in the experiment and also satisfies Shannon's sampling theorem. The boundary conditions of all nodes are simulated as all free except a fixed z direction translation of the center nodal point of section 3 to resist the rigid body motion.

2.2 Wave conversion at joints

In Fig. 2(a), a 5 kHz harmonic force was assumed to be induced in the lateral direction on beam section 1. The lateral oscillation is propagated by flexural waves from the excitation site to the joints. The analysis yields two spatial functions of particle displacements, one longitudinal and the other flexural. When the incident flexural waves in beam section 1 passes through the first joint, the amplitudes of the flexural waves in beam sections 2 and 3 are decreased because most of incident flexural wave energy is changed to the longitudinal wave in beam section 3. The longitudinal wave in beam section 3 acts as a force in the beam elements connected to the second joint. This force acts along the normal to the plane of the beam sections 4 and 5 and therefore

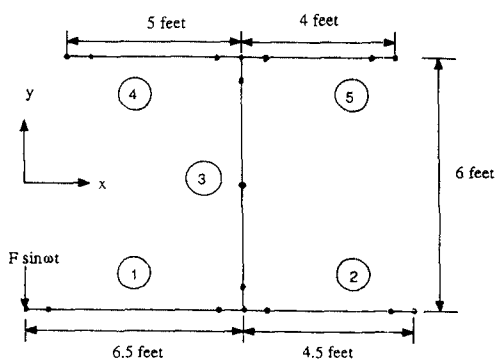

Fig. 1 Finite element modeling of the "H" frame

creates a flexural wave in beam sections 4 and 5. The transmitted flexural wave from beam section 3 has a gain in beam section 4 and a loss in beam section 5. This gain or loss depends on the material used and its physical dimensions. It is observed that the amplitudes of the flexural waves at the ends of each beam section are greater than those for the reflected waves. The greater amplitudes are effective at a wavelength distance from the beam's ends because of a nearfield effect. In Fig. 2(b), the amplitudes of the reflected and incident longitudinal waves in beam section 1 are relatively small compared to those of the incident flexural wave in beam section 1 because the small portion of incident energy of the flexural wave is reflected as a longitudinal wave at the first joint. In beam section 3, the lateral oscillation produced in beam section 1 acts as a longitudinal force to the cross beam. Therefore, there is a remarkably high transformation rate of a flexural wave into a longitudinal wave in beam section 3. In beam sections 4 and 5, most of the longitudinal wave energy in beam section 3 is converted to the flexural wave. Only the energy contained in the flexural wave in beam section 3 is utilized in increasing the amplitudes of longitudinal waves in beam sections 4 and 5.

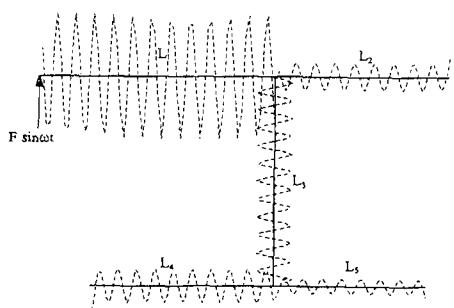

(a) flexural wave

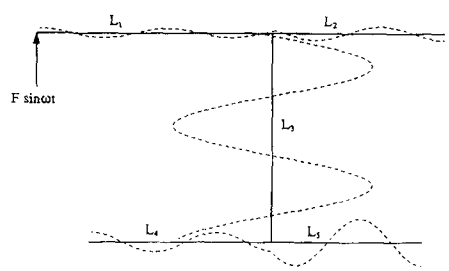

(b) longitudinal wave

Fig. 2 Distribution of the particle displacements along the "H" frame

2.3 Dispersion

The structural responses of the described system predicted by the finite element method and experiments are generally dispersive because of the dispersive nature of the flexural wave. That is, each harmonic component propagates at a different wave speed such that a wave shape is changed with time. In this context, a differentiation must be made between the phase velocity and the group velocity (Cremer, 1973).

Figure 3 shows the dispersion curves for the flexural and the longitudinal waves in frequency range 5 kHz to 10 kHz. For the flexural wave, the bending wavenumber k_B and the circular frequency ω are related by

$$k_B=\sqrt[4]{\frac{\rho A}{EI}}\sqrt{\omega},$$

where EI is the bending stiffness and ρA is the mass per unit length. The flexural wavenumber depends on the square root of the frequency. For the longitudianal wave, the wavenumber k_L and the circular frequency are related by

$$k_L=\frac{\omega}{c_L},$$

where c_L is a phase velocity of the longitudinal wave. The wavenumber k_L is the spatial analog of the circular frequency. The longitudinal wave is a straight line representing a nondispersive system, while the flexural wave has a dispersive

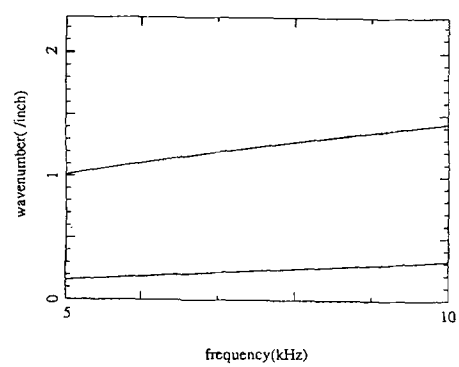

Fig. 3 Dispersion curves of the flexural and the longitudinal waves

behavior depending on $\sqrt{\omega}$. Therfore, these different dispersion behaviors are used as a spatial technique to discriminate between two different types of waves.

2.4 Numerical technique

For the finite element analysis using ANSYS, a broad band white noise from 5 kHz to 10 kHz is represented as the collection of 810 harmonic single frequencies with increment of 6.17 Hz. For every given single frequency, the displacements at each nodal point of a finite element model are calculated and then, are inputs for the FFT from the spatial domain to the wavenumber domain. Zero padded 64 data produced at nodal points on each beam section are Fourier transformed to the wavenumber domain for every 810 single frequencies. The transformed data in the wavenumber domain are symmetric about the Nyquist wavenumber $k_{\max}=2.28$/inch. In this study, only one of the two symmetric parts is employed and 810 frequency components for each of the 32 different wavenumbers are divided into 270 segments to reduce the size of the data contained in a wavenumber-frequency spectrum. Each segment contains three sequential frequency components x_n and are averaged as follows:

$$A=[\frac{1}{3}\sum_{n=1}^{3}x_n^2]^{\frac{1}{2}}, \quad n=1, 2, 3$$

Then, 270 averaged frequency components A about every 32 different wavenumbers are generated in Figs. 4 through 8.

2.5 Numerical results

In the wavenumber-frequency spectra (Figs. 4 through 8), the x-axis represents the frequency range 5 kHz to 10 kHz; the y-axis represents the wavenumber range 0 to 2.28/inch, and the z-axis represents displacements. It is observed that the peak values representing resonant frequencies in the wavenumber-frequency spectra must have infinite values, however, the peak values have finite amplitudes. There are two reasons. The one is the poor resolution in the frequency domain. The given frequencies in the range 5 kHz to 10 kHz with increment 6.17 Hz do not exactly coincide

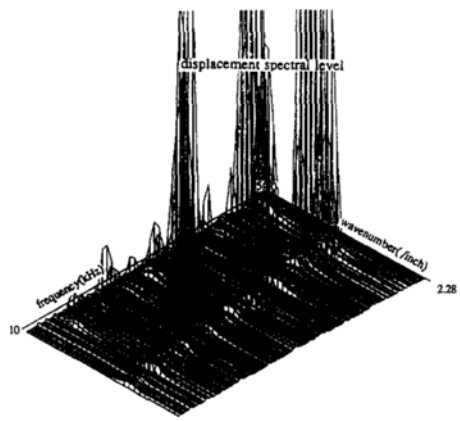

Fig. 5 Dispersion curves of the flexural and the longitudinal waves at beam section 2 of the "H" frame

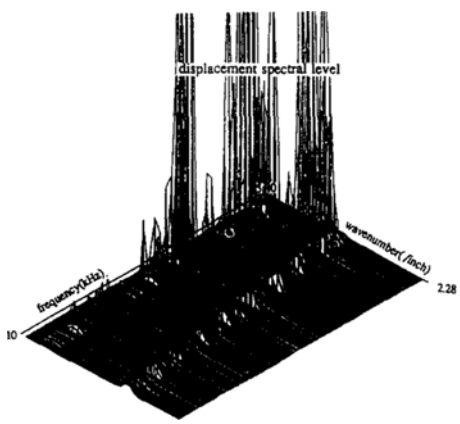

Fig. 4 Dispersion curves of the flexural and the longitudinal waves at beam section 1 of the "H" frame

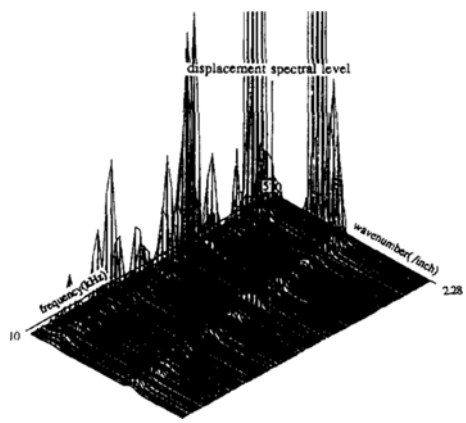

Fig. 6 Dispersion curves of the flexural and the longitudinal waves at beam section 3 of the "H" frame

with the natural frequencies of a system. The other reason is that the averaged three sequential frequency components about every 32 different wavenumbers make the peak values have finite amplitudes. It is observed that the energy of the wavenumber-frequency components leaks into the adjoining spectral lines. This is a leakage which comes from poor resolution in wavenumber and frequency domains and an unperiodic sampling window for the FFT.

As predicted in Fig. 3, the flexural and the longitudinal wave dispersion curves are identical to those in Figs. 4 through 8. Figures 4 through 8 represent the flexural and the longitudinal wave dispersion curves at each section of a system when the flexural direction harmonic forces are induced at the end of beam section 1. It is observed that overall amplitudes of the flexural waves in beam section 1 are decreased in beam section 3 because most flexural wave energy is changed to the longitudinal waves in beam section 3. There are losses in sections 4 and 5 when the flexural and longitudinal waves pass through the second joint.

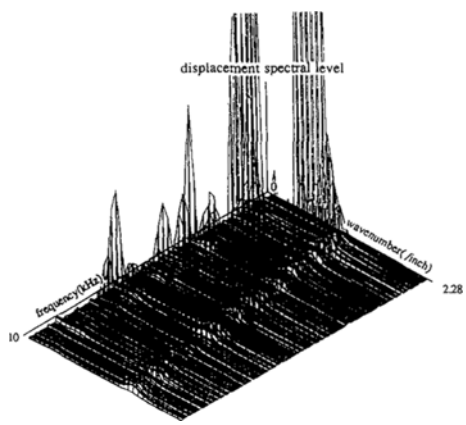

Fig. 7 Dispersion curves of the flexural and the longitudinal waves at beam section 4 of the "H" frame

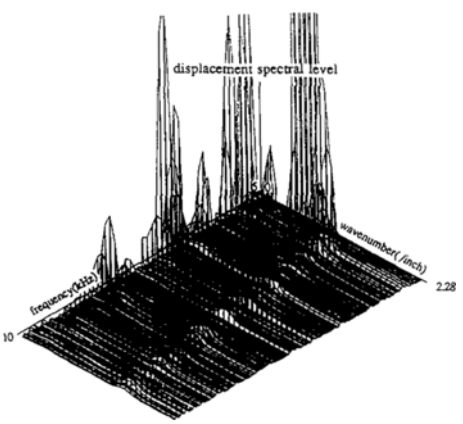

Fig. 8 Dispersion curves of the flexural and the longitudinal waves at beam section 5 of the "H" frame

3. Experimental Analysis

3.1 Laboratory set-up

The laboratory set-up used was designed to model a finite beam system. The experimental model consists of two parallel finite rectangular steel beams welded rigidly by a cross rectangular steel beam with cross-sectional dimensions of 2 inches by 0.5 inches. Free boundary conditions are simulated of all ends of the described system. The "H" frame is supported at five points with thin steel wires which are able to be individually adjusted vertically. The "H" frame was excited by a shaker driving through a thin rod at the end of beam section 1.

3.2 Theory of accelerometer array

Use of an accelerometer array technique is important to spatial signal processing to prevent aliasing about the highest wavenumber. This technique is similar to that proposed to measure the wall pressure in a turbulent boundary layer, as has been discussed by Hodgson and Keltie(1984). In the present study this technique was adopted to take experimental data using twenty three accelerometers.

Consider that the responses of the accelerometers, $U_n(x_n\,;\,t)$, are sampled from N equally spaced accelerometers mounted on a beam in one coordinate direction at a distance h apart. Let the output of a finite time interval $t=0$ to $t=M\Delta t$ be Fourier transformed to the frequency domain producing M outputs, $U_n(x_n\,;\,\omega)$ from each of the spatial sampling points at $x_n=nh$, $n=0,\ 1,\ \cdots,\ N-1$. Each of these data may be Fourier transformed to the wavenumber domain to yield $N/2$ independent spectral lines, $U_n(k_n\,;\,\omega)$, in the wavenumber domain. These spectral

lines are given at this discrete wavenumber

$$k_m=\frac{2\pi m}{Nh};\ m=0,1,\ \cdots,\ \frac{N}{2}-1.$$

The highest wavenumber associated with the accelerometer spacing h according to the relation

$$k_{\max}=\frac{\pi}{h},$$

where $k_{\max}$, is called the Nyquist wavenumber. These results are shown from the sampling theorem in the spatial domain which states that at least two samples per wavelength are required to define a wavenumber component in the original data. Hence the sampling rate should be at least two times of the highest wavenumber.

The resolution of the $N/2$ spectral lines will be

$$\Delta k=\frac{2\pi}{Nh}.$$

Thus, for a given value of h, as the number of accelerometers increases, the number of spectral estimates also increase and the resolution bandwidth decreases.

3.3 Transfer function correction technique

As depicted in Fig. 9, all twenty three accelerometer were mounted on the electrodynamic shaker head with a broad band white noise input from 5 kHz to 10 kHz to measure the electronically introduced magnitude and phase differences. With this arrangement, each accelerometer was subjected to the same excitation in both phase and magnitude. As the accelerations are converted to voltages, each acceleration, S, is effectively multiplied by the overall complex gain. For example, performing the transfer function on two signals is equal to the ratio of the cross-spectrum between transducers 0 and 1 to the power-spectrum of transducer 0. The relative phase between transducers 0 and 1 can be obtained inverse tangent of the ratio of the imaginary part of the cross-spectrum to the real part of the cross-spectrum between transducers 0 and 1. In this way, the complex gain and the phase difference about a master channel (in this case channel 0) may be compared to the other twenty two channels.

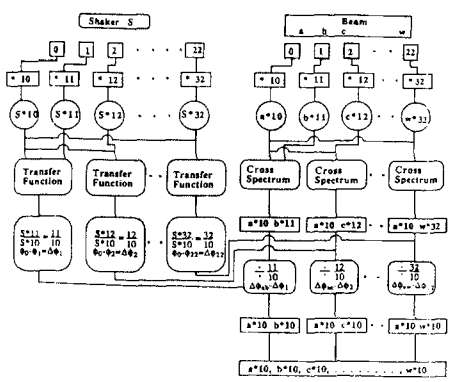

Fig. 9 Schematic diagram of transfer function correction technique

The 23 accelerometers are mounted on each beam section of an "H" frame and measure the accelerations through the transducers. The accelerations are again multiplied by the complex gain of each channel. The cross-spectrum is equivalent to multiplying complex signals. Thus, the cross-spectrum of two accelerometers is then the acceleration at the reference point multiplied by a complex instrument gain times the acceleration at the other point multiplied by a complex instrument gain. If the cross-spectrum of a pair is divided by the transfer function when a pair was mounted on the shaker, the result is equivalent to the product of both acceleration in the pair multiplied by the same instrument gain. The phase error can also be compensated by subtracting the relative phase difference from channel 1. In this way, phase and gain differences between instrument channels in a pair can be eliminated.

3.4 Experimental technique

This study investigates the wave transmission through two "T" joints using 23 accelerometers. The signals taken at 23 different locations during two seconds on each beam section using the accelerometers are sampled simultaneously by sample-and-hold modules in MASSCOMP at a sampling rate of 38 kHz. Then the first 8192 data points of 22 pair channels (a master channel with the other 22 channels) are Fourier transformed and combined to make the cross-spectrum. Using the cross-spectra for each pair of channels and the transfer function, the corrected magnitude and phase for each channel can be obtained. Next, another 8192 data points are selected, the first half of which include the previous data set. The

magnitude and phase correction procedure is repeated on this data set. This is repeated 16 times to obtain the entire averaged data. The obtained 8192 averaged data points at 23 different locations represent frequency components from 0 Hz to 19 kHz with increments of 4.64 Hz. However, we need the frequency components in the range 5 kHz to 10 kHz. The data in this frequency range locate from the 1078th to 2157th components among 8192 averaged frequency components. Therefore, 1080 frequency components at 23 different locations are obtained. For characterizing the data in the wavenumber-frequency domain, the data in the spatial domain for every 1080 single frequencies must be Fourier transformed to the wavenumber domain. For the FFT, a number of spatial domain data requires a power of 2. Therefore, the 23 spatial domain data for every 1080 single frequencies are padded with zeros up to a 64 data sequence in order to make the same interpolation width as the analytical results. The transformed data in the wavenumber domain are symmetric about the Nyquist wavenumber $k_{max}=$ 2.28/inch. In this study, only one of the two symmetric parts is employed and 1080 frequency components for each of the 32 different wavenumbers are divided into 270 segments to reduce the size of the data contained in a wavenumber-frequency spectrum. Each segment contains four sequential frequency components x_n and are averaged as follows :

$$A=\left[\frac{1}{4}\sum_{n=1}^{4}x_n^2\right]^{\frac{1}{2}}, \quad n=1, 2, 3, 4$$

Then, 270 averaged frequency components A about every 32 different wavenumbers are generated in Figs. 10 through 14.

3.5 Experimental results

In the wavenumber-frequency spectra (Figs. 10 through 14), the x-axis represents the frequency range 5 kHz to 10 kHz ; the y-axis represents the wavenumber range 0 to 2.28/inch, and the z-axis represents acceleration spectral level. It is observed that the energy of wavenumber-frequency components leaks into the adjoining spectral lines. This is a leakage which comes from poor resolution in wavenumber and frequency domains

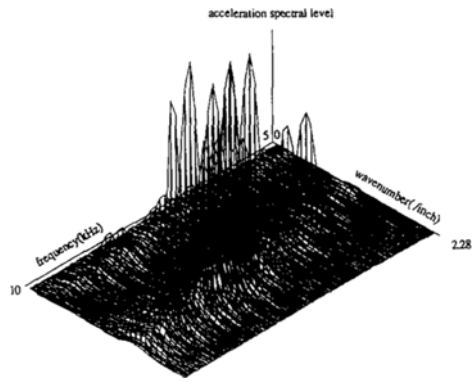

Fig. 10 Dispersion curves of the flexural and the longitudinal waves at beam section 1 of the "H" frame

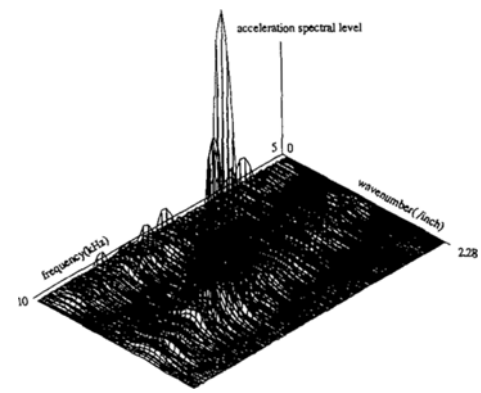

Fig. 11 Dispersion curves of the flexural and the longitudinal waves at beam section 2 of the "H" frame

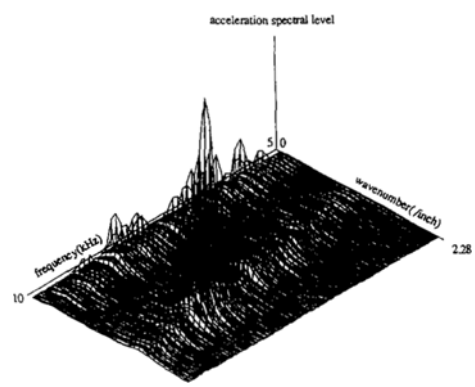

Fig. 12 Dispersion curves of the flexural and the longitudinal waves at beam section 3 of the "H" frame

and an unperiodic sampling window for the FFT. In the wavenumber-frequency spectrum, the peak values representing the resonant frequencies do not occur at the same frequencies in all five beam sections because the local resonances of each beam section depend on the dimensions of the beam. As predicted in Fig. 3, the flexural and the longitudinal wave dispersion curves are identical to those in Figs. 10 through 14.

Figures 10 through 14 represent the flexural and the longitudinal wave dispersion curves at each section of a system when a broad band white noise from 5 kHz to 10 kHz is induced in the flexural direction at the end of beam section 1. There is a remarkably high transformation rate of a flexural waves into longitudinal waves in beam section 3. Therefore, the overall amplitudes of the transmitted flexural waves in beam section 3 are relatively small compared to those in beam section 1. There are losses in beam sections 4 and 5. Only a small portion of energy of the longitudinal and flexural waves in beam section 3 is transmitted to beam sections 4 and 5.

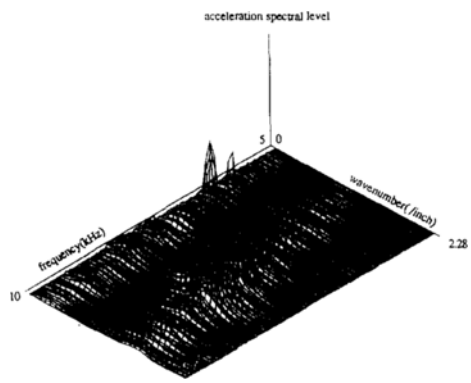

Fig. 13 Dispersion curves of the flexural and the longitudinal waves at beam section 4 of the "H" frame

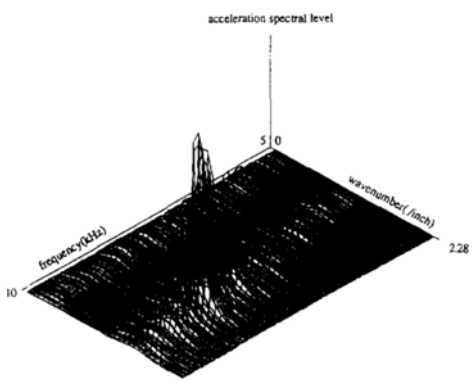

Fig. 14 Dispersion curves of the flexural and the longitudinal waves at beam section 5 of the "H" frame

4. Comparison between the Numerical and the Experimental Results

The overall energy level was obtained by the root mean square of the overall wavenumber-frequency components of the flexural and the longitudinal waves separately at each beam section. For the numerical results, a reference energy level is chosen as the root mean squared wavenumber-frequency components of the longitudinal waves in beam section 1. The root mean squared wavenumber-frequency components of the flexural and the longitudinal waves in the other sections are divided by the reference energy level to obtain all relative values. As the same

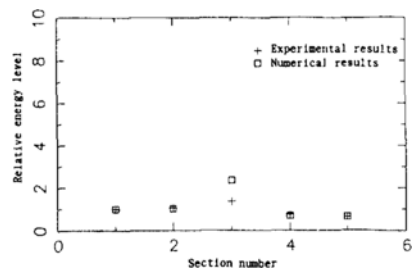

(a) Relative energy level of the longitudinal waves

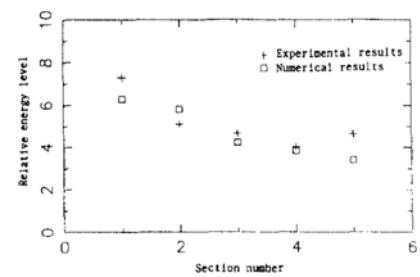

(b) Relative energy level of the flexural waves

Fig. 15 The relative energy level of the longitudinal and the flexural waves

manner in the experimental results, the reference energy level is chosen as the root mean squared wavenumber-frequency components of the longitudinal waves in the beam section 1. All relative values about the reference energy level are obtained the same as in the previous case.

Figure 15 compares the obtained relative values of the numerical and the experimental results. Figure 15(a) shows the relative values of the longitudinal waves at each section. The relative value of the longitudinal waves in section 3 by the numerical analysis is 70% higher than that by the experiment.

Figure 15(b) shows the relative values of the flexural waves at each section. The overall energy level of the flexural waves in beam section 1 is approximately 6 or 7 times higher than that of the longitudinal waves in beam section 1. The overall energy level of the flexural waves has a loss in sections 2 and 3 because most flexural waves changes to the longitudinal waves in beam section 3.

Comparisons between the numerical analysis and the experiment show a good agreement. Therefore, reasonable prediction of wave transmission under certain classes of structure and design circumstance may be obtained by the technique demonstrated in this study.

5. Conclusions

The analysis presented in this study shows that joints cause a change in the type of waves reflected and transmitted. It is also observed that there is either a gain or a loss in the amplitudes of the flexural waves during transmission through the second joint. This loss or gain in beam sections 4 and 5 depends on the material used and physical dimensions of beams. In spite of the limited wavenumber resolution, the experimental results from the 23 channel input limitation of the system provided reasonable prediction of wave transmission through two "T" joints. Even though the difference of rms values of the overall wavenumver-frequency components of the flexural and longitudinal waves at each beam section between the numerical and the experimental results is significant in section 3, the trends of increased and decreased energy of the flexural and longitudinal waves before and after the joints show good agreement between the numerical and the experimental results.

References

Bhattacharya, M. and Mulholland, K., 1971, "Propagation of Sound Energy by Vibration Transmission via Structural Junctions," J. Sound Vib., Vol. 18, pp. 221~234.

Blake, W. and Chase, D., 1971, "Wavenumber-Frequency Spectra of Turbulent Boundary Layer Pressure Measured by Microphone Arrays," J. Acoust. Soc. Am., Vol. 49, No. 3, pp. 862~877.

Bull, M., 1967, "Wall-Pressure Fluctuations Associated with Subsonic Turbulent Boundary Layer Flow," J. Fluid Mech., Vol. 28, pp. 719~754.

Cremer, L., Heckl, M. and Unger, E.E., 1973, *Structure Borne Sound,* Springer Verlag, Berlin, p. 280.

Doyle, J. F. and Kamle, 1987, "An Experimental Study of the Reflection and Transmission of Flexural Waves at an Arbitrary T-Joint," J. Appl. Mech., Vol. 54, pp. 136~140.

Hodgson, T. and Keltie, R., 1984, "An Innovative Fast Fourier Transform Array Technique for Low Wavenumber Measurements of the Turbulent Boundary Layer Fluctuating Pressure Field," Symposium on Flow-Induced Vibrations, Vol. 5, pp. 39~51.

Gaul, L., 1983, "Wave Transmission and Energy Dissipation at Structural and Machine Joints, Trans. ASME, Series L, Vol. 105, pp. 489~496.

Lyon, R., 1975, *Statistical Energy Analysis of Dynamic Systems*. The MIT Press, Massachusetts.

Maidanik, G. and Jorgensen, D., 1967, "Boundary Wave-Vector Filters for the Study of the Pressure Field in a Turbulent Boundary Layer," J. Acoust. Soc. Am., Vol. 42, No. 2, pp. 494~501.

Rosenhouse, G., 1970, "Acoustic Wave Propagation in Bent Thin-Walled Wave Guides," J. Sound Vib., Vol. 67, pp. 469~486.

Wills, J., 1970, "Measurements of the

Wavenumber/Phase Velocity Spectrum of Wall Pressure beneath a TBL," J. Fluid Mech., Vol. 45, pp. 65~90.

Yoshimura, M., 1977, "Measurement of Dynamic Rigidity and Damping Property of Simplified Joint Models and Simulation by Computer," Annals of the CIRP, Vol. 25, No. 1, pp. 193~198.

Yoshimura, M., 1979, "Computer-Aided Design Improvement of Machine Tool Structure Incorporating Joint Dynamic Data," Annals of the CIRP, Vol. 28, No. 1, pp. 241~246.